Geomechanics and Engineering, *Vol. 16, No. 6 (2018) 577-588*
DOI: https://doi.org/10.12989/gae.2018.16.6.577

MARS inverse analysis of soil and wall properties for braced excavations in clays

Wengang Zhang[*1,2,3], Runhong Zhang[2] and Anthony. T. C. Goh[4]

[1]*Key Laboratory of New Technology for Construction of Cities in Mountain Area, Chongqing University, Chongqing 400045, China*
[2]*School of Civil Engineering, Chongqing University, Chongqing 400045, China*
[3]*Key Laboratory of Rock Mechanics in Hydraulic Structural Engineering, Ministry of Education, Wuhan University, Wuhan 430072, China*
[4]*School of Civil and Environmental Engineering, Nanyang Technological University, 639798, Singapore*

(Received August 29, 2016, Revised July 19, 2017, Accepted October 12, 2018)

Abstract. A major concern in deep excavation project in soft clay deposits is the potential for adjacent buildings to be damaged as a result of the associated excessive ground movements. In order to accurately determine the wall deflections using a numerical procedure such as the finite element method, it is critical to use the correct soil parameters such as the stiffness/strength properties. This can be carried out by performing an inverse analysis using the measured wall deflections. This paper firstly presents the results of extensive plane strain finite element analyses of braced diaphragm walls to examine the influence of various parameters such as the excavation geometry, soil properties and wall stiffness on the wall deflections. Based on these results, a multivariate adaptive regression splines (MARS) model was developed for inverse parameter identification of the soil relative stiffness ratio. A second MARS model was also developed for inverse parameter estimation of the wall system stiffness, to enable designers to determine the appropriate wall size during the preliminary design phase. Soil relative stiffness ratios and system stiffness values derived via these two different MARS models were found to compare favourably with a number of field and published records.

Keywords: wall deflection; braced excavation; soil stiffness ratio; case histories; multivariate adaptive regression splines; inverse analysis

1. Introduction

Within a built-up environment, the construction safety of a deep excavation becomes more crucial with the ever-increasing building density. It is of vital importance to predict and control the ground movement of a deep excavation during construction to ensure the minimal structural damage to nearby buildings and utilities. For excavations in ground that comprises of thick soft clays overlying stiff clay,braced walls are usually used to minimize ground movements. It is common to extend the wall

length into the stiff clay layer to prevent basal heave failure and to reduce the movement of the wall toe. To ensure the serviceability limit state is satisfied, a common design criterion is to limit the maximum wall deflection to a fraction of the excavation depth, typically in the range of 0.5% to 1.5% of H_e. Unnecessarily severe restrictions may lead to uneconomic design. Therefore, reliable estimates of wall deflections under working conditions are essential.

Numerical tools such as the finite element method are increasing being used to analyze deep excavation problems. They can provide a better understanding of soil behaviour during construction, verify the performance of complex excavations through comparison with field observations, and even predict future responses. Nevertheless, accurate prediction of deformations induced by deep excavations using numerical approaches is still rather complicated for engineers since apart from modelling the actual construction sequence and wall system parameters, reliable information on selection of constitutive models and the appropriate soil parameters are also required. Although comprehensive laboratory and field tests can be conducted, there are still some difficulties in the precise determination of some of the soil parameters such as the soil stiffness because of sample disturbance and testing errors. Furthermore, even with well-measured soil parameters, the estimated performance may still deviate from the field observation as a result of the inherent spatial variability and inadequacy of the simulation model itself (Zhao *et al.* 2015). Therefore inverse analysis can play a vital role to estimate the relevant soil parameters for more reliable predictions of the expected wall and ground movements that are induced during excavation. Inverse analysis involves utilizing field measurements in order to obtain soil material parameters in contrast to the conventional forward approach. A forward analysis starts with the determination of a constitutive model and its associated parameters derived from laboratory and field testing or empirical relationships. These parameters are then adopted as inputs for numerical analysis to predict stresses, strains, displacements, etc. Previous applications of inverse analyses in geomechanics for soil parameter identification

∗Corresponding author, Professor
E-mail: cheungwg@126.com

ISSN: 2005-307X (Print), 2092-6219 (Online)

include Gioda (1985), Zentar *et al.* (2001), Lecampion *et al.* (2002), Calvello and Finno (2004), Finno and Calvello (2005), Miranda (2007), Levasseur *et al.* (2008), Rechea *et al.* (2008), Yan *et al.* (2009), Papon *et al.* (2011), Chiu *et al.* (2012) and Moreira *et al.* (2013). Optimization algorithms including the gradient based, artificial neural networks and the genetic algorithms are commonly adopted to derive these parameters.

When applying inverse analysis techniques to study the behaviour of an actual supported excavation, concerns arise about the proper representation of the real system, as well as the efficiency of the inverse analysis technique and its ability to find a unique set of parameters for a particular geological subsurface. Inverse analyses of supported excavation systems has been carried out by a number of researchers including Ou and Tang (1994), Calvello and Finno (2004), Finno and Calvello (2005), Levasseur *et al.* (2008), Levasseur *et al.* (2010), Hashash *et al.* (2010), Juang *et al.* (2013) and Moreira *et al.* (2013).

Deep excavations in thick deposits of soft clay can cause excessive ground movements and result in damage to adjacent buildings. Numerical analysis using the finite element method to estimate wall deflections for braced excavations can often differ from the values measured in the field. This can be due to many uncertainties with regard to the true soil properties during the preliminary design phase. The use of inverse analysis based on field measurements of wall deflections is therefore a useful technique to infer the correct soil material response, which subsequently can be used to improve the numerical predictions for forward analysis of subsequent excavation stages and for future projects in similar soil conditions.

Firstly a series of parametric studies were carried out using the plane strain finite element (FE) software Plaxis (Brinkgreve *et al.* 2006) in which the soft clay stress-strain behavior was modeled using the hardening small strain (HSS) constitutive relationship that considers the small strain effect. Analyses were carried out to examine the wall deflections with regard to a number of parameters including the excavation geometry, soil strength and stiffness properties, and the wall stiffness. Based on these results, a multivariate adaptive regression splines approach was developed for inverse parameter identification of the soil relative stiffness ratio. A second MARS model was also developed for inverse parameter estimation of the wall system stiffness, to enable designers to determine the appropriate wall size during the preliminary design phase. Soil relative stiffness ratios and system stiffness values derived via this MARS method were found to compare favourably with a number of field and published records.

2. MARS methodology

Similar with the traditional nonlinear regression modelling techniques (Zhang and Goh 2015a, Zhang *et al.* 2015, Zhang *et al.* 2016, Zhang and Goh 2016, Ji *et al.* 2016), MARS is nonlinear and nonparametric method for fitting the relationship between a set of input variables and dependent variables in high dimensional data (Friedman 1991). The method adopts a divide-and-conquer strategy in

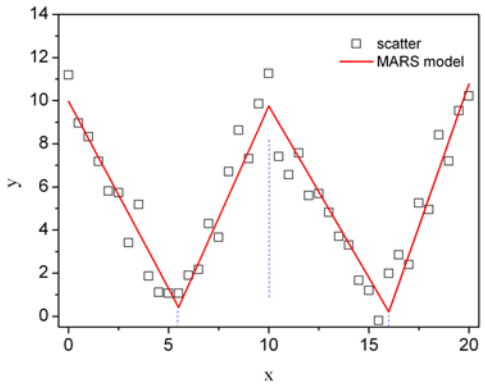

Fig. 1 Knots and linear splines for a simple MARS example

which the training data sets are partitioned into separate piecewise linear segments (splines) of differing gradients (slope). No specific assumption about the underlying functional relationship between the input variables and the output is required. The end points of the segments are called knots. A knot marks the end of one region of data and the beginning of another. The resulting piecewise curves (known as basis functions), give greater flexibility to the model, allowing for bends, thresholds, and other departures from linear functions. An open source code on MARS from Jekabsons (2010) is used in carrying out the analyses presented in this paper.

The MARS model *f(X)*, is constructed as a linear combination of basis functions (BFs) and their interactions, and is expressed as

$$f(X) = \beta_0 + \sum_{m=1}^{M} \beta_m \lambda_m(X) \tag{1}$$

where each $\lambda_m(X)$ is a basis function. It can be a spline function, or the product of two or more spline functions already contained in the model (higher orders can be used when the data warrants it; for simplicity, at most second-order is assumed in this paper). The coefficients β are constants, estimated using the least-squares method.

BFs are splines (smooth polynomials), including piecewise linear and piecewise cubic functions. For simplicity, only the piecewise linear function is expressed. Piecewise linear functions are of the form $\max(0,x-t)$ with a knot occurring at value t. The equation max(.) means that only the positive part of (.) is used otherwise it is given a zero value. Formally,

$$\max(0, x-t) = \begin{cases} x-t, if\ x \geq t \\ 0, otherwise \end{cases} \tag{2}$$

Fig. 1 shows a simple example of how MARS would use piecewise linear spline functions to attempt to fit data. The MARS mathematical equation is expressed as

$$y = -44.08 + 4.24 \times BF1 - 3.67 \times BF2 + 6.31 \times BF3 - 2.50 \times BF4 \tag{3}$$

where $BF1 = \max(0, 16 - x)$, $BF2 = \max(0, x - 10)$, $BF3 = \max(0, x - 5.5)$ and $BF4 = \max(0, 5.5 - x)$. The knots are located at x = 5.5, 10 and 16. They delimit four intervals where different linear relationships are identified.

MARS generates basis functions by searching in a stepwise manner. It searches over all possible univariate knot locations and across interactions among all variables. An adaptive regression algorithm is used for selecting the knot locations. MARS models are constructed in a two-step procedure. The forward phase adds functions and finds potential knots to improve the performance. This continues until the model reaches some predetermined maximum number of terms, resulting in a purposely overfitted model. Subsequently, to prevent overfitting, the backward phase prunes the least effective terms based on the Generalized Cross-Validation (GCV) method. The GCV equation is a goodness of fit test that penalizes large numbers of BFs and serves to reduce the chance of overfitting. For the training data with N observations, GCV for a model is calculated as follows (Hastie *et al.* 2009)

$$GCV = \frac{\frac{1}{N}\sum_{i=1}^{N}[y_i - f(x_i)]^2}{[1-\frac{M+d\times(M-1)/2}{N}]^2} \quad (4)$$

in which M is the number of BFs, d is the penalizing parameter, representing a cost for each basis function optimization and is a smoothing parameter of the procedure. Larger values for d will lead to fewer knots being placed and thereby smoother function estimates. According to Friedman (1991), the optimal value for d is in the range $2 \leqq d \leqq 4$ and generally the choice of $d = 3$ is fairly effective. In this study, a default value of 3 is assigned to the penalizing parameter d. N is the number of observations, and $f(x_i)$ denotes the predicted values of the MARS model. At each deletion step a basis function is removed to minimize Eq. (1), until an adequate fitting model is found. MARS is an adaptive procedure because the selection of BFs and the variable knot locations are data-based and specific to the problem at hand.

The MARS modeling is a data-driven process. After the optimal MARS model is determined, by grouping together all the BFs that involve one variable and another grouping of BFs that involve pairwise interactions (and even higher level interactions when applicable), the procedure known as analysis of variance (ANOVA) decomposition (Friedman 1991) can be used to assess the contributions from the input variables and the BFs through comparing (testing) variables for statistical significance. Previous applications of MARS algorithm in civil engineering can be found in Attoh-Okine *et al.* (2009), Lashkari (2012), Mirzahosseinia *et al.* (2011), Zarnani *et al.* (2011), Samui (2011), Samui and Karup (2011), Zhang and Goh (2013, 2014, 2015, 2016a, b), Goh and Zhang (2014), Goh *et al.* (2016, 2017), Zhang and Goh (2018), Goh *et al.* (2018).

3. Finite element analyses

The database used for the MARS analyses were based on plane strain finite element forward analyses of the maximum wall deflection for multi-strutted diaphragm walls as described in detail in Zhang *et al.* (2015). Fig. 2 presents the cross-sectional soil and wall profile considered. The parameters that were considered were: excavation

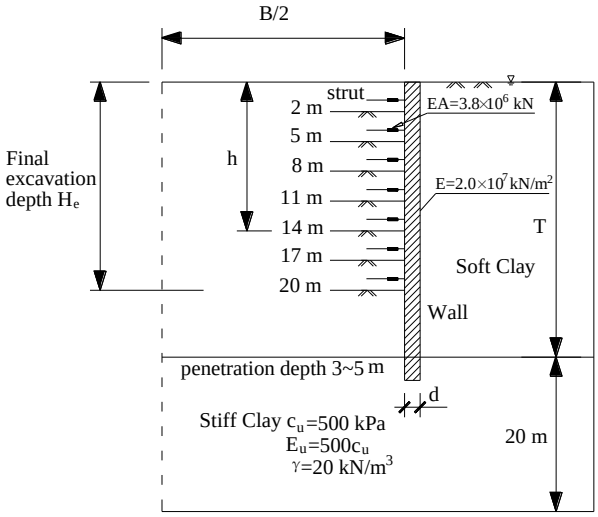

Fig. 2 Cross-sectional soil and wall profile

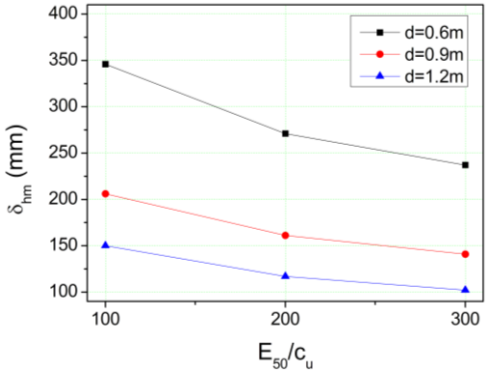

(a) $c_u/\sigma'_v = 0.25$

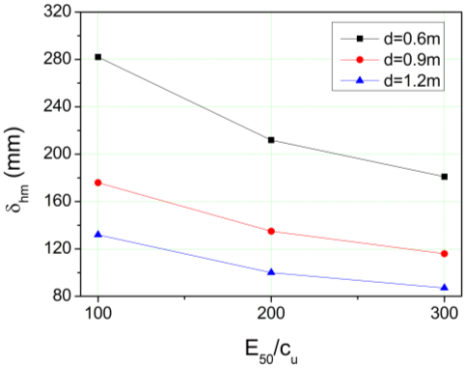

(b) $c_u/\sigma'_v = 0.29$

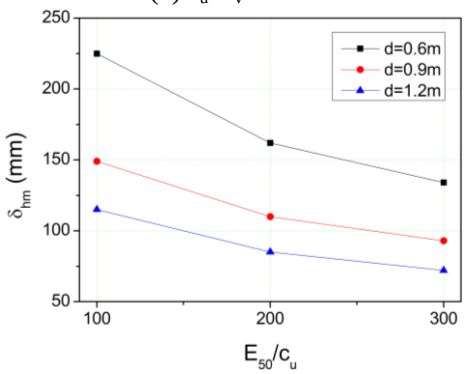

(c) $c_u/\sigma'_v = 0.34$

Fig. 3 Effect of soil stiffness on wall deflection for H_e = 20 m (γ= 17 kN/m^3, B = 30 m, T = 30 m)

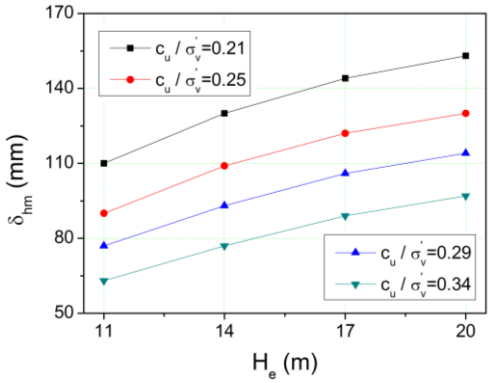

Fig. 4 Effect of soil shear strength ratio on wall deflection for d = 1.2 m (γ= 17 kN/m^3, B = 40 m, E_{50}/c_u = 200, T = 30 m)

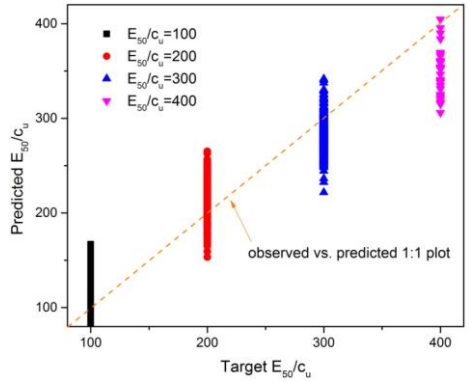

Fig. 5 Observed vs. predicted 1:1 plots of E_{50}/c_u

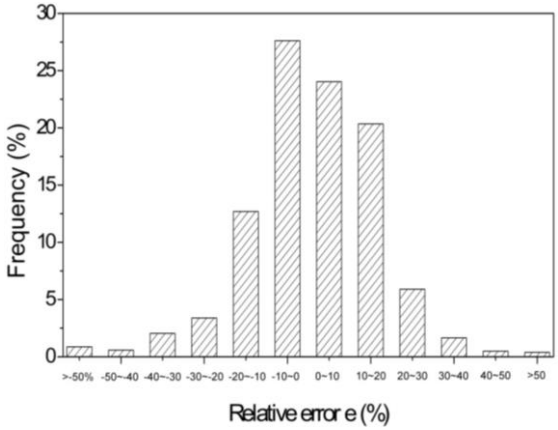

Fig. 6 Histogram of relative errors for the MARS E_{50}/c_u model

width B; excavation depth H_e; soft clay thickness T; soil unit weight γ; the system stiffness $\ln(S)$ [$S = EI/\gamma_w h_{avg}^4$), as defined in Clough and O'Rourke (1990), where E is the Young's modulus of wall material, I is the moment of inertia of the wall section, γ_w is the unit weight of water, and h_{avg} is the average spacing of the struts]; the relative soil shear strength ratio c_u/σ'_v, where c_u is the undrained shear strength and σ'_v denotes the vertical effective stress; and the relative soil stiffness ratio E_{50}/c_u, where E_{50} is the secant stiffness in standard drained triaxial test.

A total of 1032 cases were considered, based on parameter combinations of the seven design variables. The influence of the soil stiffness ratio E_{50}/c_u on the maximum wall deflection is shown in Figure 3a-c for cases with γ= 17 kN/m^3, B = 30 m, and T = 30 m for c_u/σ'_v = 0.25, 0.29, and 0.34, respectively. It is obvious that the wall deflection decreases with the increase of the relative soil stiffness ratio E_{50}/c_u. In addition, the influence of E_{50}/c_u is more significant for walls of lower thickness d. The influence of the soil shear strength ratio c_u/σ'_v is presented in Fig. 4, for the cases with γ =17 kN/m^3, B = 40 m, d = 1.2 m, E_{50}/c_u = 200 and T = 30 m. The results show the maximum wall deflection decreases with the increase of the soil shear strength ratio.

Analyses indicated that the maximum wall deflections decrease almost linearly with decreasing ground water level and that the water table correction factor μ_w can be approximated as $\mu_w = 1 - 0.1l$, where l is the depth of the ground water table below the ground surface (in meters) and $l \leqq 2$. Thus, the wall deflection δ_h^* can be derived from

$$\delta_h^* = \delta_{h,M}/\mu_w \quad (5)$$

in which $\delta_{h,M}$ is the maximum of wall deflection for the case with the ground water table at the ground surface.

4. MARS model for E_{50}/c_u

Based on the forward analysis results described in the previous section, a MARS model has been developed for inverse analysis to estimate the soil relative stiffness ratio E_{50}/c_u as a function of seven input parameters: γ, B, H_e, c_u/σ'_v, δ_h^*, $\ln(S)$, and T. Herein the measured wall deflection δ_h^* is used as an input parameter to back-calculate E_{50}/c_u.

The dataset was separated randomly into a training set of 775 patterns and a testing set of 257 patterns. The MARS model with the highest R^2 value and less BFs for the testing data set is considered to be the optimal. The optimal MARS model adopted 28 BFs of linear spline functions. The observed versus predicted 1:1 plots of E_{50}/c_u are shown in Fig. 5. The developed model predicts slightly higher estimations for low E_{50}/c_u values and slightly lower estimations for higher values of E_{50}/c_u. Fig. 6 presents the histogram plots of the relative errors e (defined as the ratio of the difference between the MARS predicted and the target E_{50}/c_u to the target value, in percentage). It is obvious that most of the MARS estimations of the data patterns fell within ±20% of the target values. In addition, it should be noted that MARS predictions still have a large range of variations with respect to the same group of targets. On the other hand, it can be acceptable since the target outputs are of category nature (types) while the estimations based on the developed model are numerical values. Some typical training and testing data sets together with the MARS predictions are listed in Tables 1 and 2, respectively.

Table 3 displays the ANOVA decomposition of the developed MARS model. The first column lists the ANOVA function number. The second column gives an indication of the importance of the corresponding ANOVA function, by

Table 1 Some typical training data for MARS E_{50}/c_u identification model

B (m)	T (m)	H_e (m)	c_u/σ'_v	δ_h^* (mm)	ln(S)	γ (kN/m^3)	Target E_{50}/c_u	MARS predicted E_{50}/c_u
30	30	11	0.34	26	8.846	19.0	400	390
30	30	11	0.34	35	7.313	19.0	400	405
40	25	14	0.34	48	8.176	19.0	300	281
30	25	20	0.34	70	7.313	17.0	300	280
40	25	20	0.25	76	8.176	19.0	300	274
30	30	20	0.29	77	8.176	19.0	300	286
30	30	20	0.34	77	7.313	19.0	300	300
40	25	20	0.25	98	7.313	19.0	300	281
40	30	20	0.29	98	8.176	17.0	300	283
30	30	11	0.29	54	7.313	19.0	300	303
40	25	14	0.29	69	8.176	19.0	200	211
40	35	20	0.34	100	8.176	19.0	200	201
50	25	20	0.34	101	7.313	17.0	200	232
30	30	20	0.34	101	8.176	15.0	200	229
40	30	17	0.34	92	8.176	15.0	300	287
40	30	20	0.21	115	8.846	19.0	200	215
50	25	14	0.29	81	8.176	17.0	200	210
40	35	14	0.34	81	6.097	19.0	300	313
40	30	17	0.34	99	8.176	19.0	100	102
40	30	17	0.21	107	8.846	19.0	200	225
40	30	17	0.29	108	8.176	15.0	300	291
30	30	20	0.25	134	8.176	15.0	200	224
40	30	11	0.25	74	8.176	17.0	300	290
40	30	20	0.34	135	7.313	15.0	300	260
30	30	20	0.29	135	7.313	17.0	200	208
30	30	20	0.34	298	6.097	15.0	100	101
40	30	20	0.25	293	6.097	17.0	200	200
50	35	14	0.29	204	6.097	17.0	200	219
40	35	11	0.25	159	7.313	19.0	100	87
50	25	11	0.25	150	7.313	17.0	100	95

Table 2 Some typical testing data for MARS E_{50}/c_u identification model

B (m)	T (m)	H_e (m)	c_u/σ'_v	δ_h^* (mm)	ln(S)	γ (kN/m^3)	Target E_{50}/c_u	MARS predicted E_{50}/c_u
30	30	11	0.29	37	8.176	19.0	400	395
40	30	11	0.34	42	8.176	19.0	300	326
40	25	17	0.34	65	8.176	19.0	200	207
30	30	14	0.34	55	7.313	19.0	300	290
60	30	14	0.29	76	8.846	17.0	200	246
40	30	20	0.25	115	8.176	17.0	300	269
30	30	17	0.25	98	8.176	19.0	200	230
40	25	20	0.29	119	6.097	19.0	300	276
30	30	17	0.34	112	7.313	15.0	300	263
40	30	20	0.25	132	8.176	15.0	300	275
40	25	17	0.34	114	7.313	19.0	100	114

Table 2 Continued

B (m)	T (m)	H_e (m)	c_u/σ'_v	δ_h^* (mm)	ln(S)	γ (kN/m^3)	Target E_{50}/c_u	MARS predicted E_{50}/c_u
30	30	17	0.29	125	8.176	17.0	100	102
30	30	17	0.34	167	6.097	19.0	100	87
40	30	14	0.29	138	6.097	19.0	200	211
30	25	11	0.29	110	6.097	17.0	200	207
50	25	11	0.29	74	7.33	17.0	300	293

Table 3 ANOVA decomposition for MARS E_{50}/c_u model

Function	GCV	STD	#basis	Variable(s)
1	1711.6	23.61	2	B
2	4915.2	58.34	2	T
3	5724.9	54.83	2	H_e
4	9107.5	54.66	2	c_u/σ'_v
5	25614.0	134.44	2	δ_h^*
6	12670.7	98.30	2	ln(S)
7	2584.5	37.73	2	γ
8	1290.3	19.34	2	T & H_e
9	1027.5	12.38	2	T & c_u/σ'_v
10	944.8	8.98	2	T & γ
11	955.4	9.62	2	H_e & ln(S)
12	1029.3	12.46	2	c_u/σ'_v & ln(S)
13	1289.3	17.04	1	δ_h^* & ln(S)
14	983.2	10.42	1	δ_h^* & γ
15	1355.8	20.12	2	ln(S) & γ

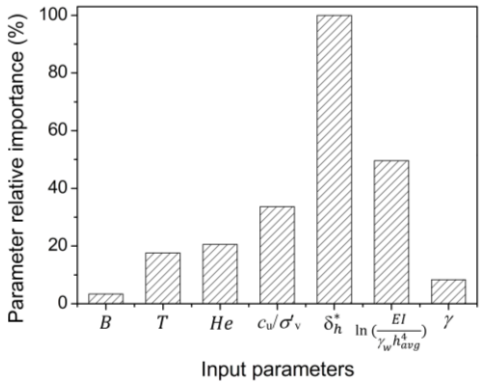

Fig. 7 Relative importance of the input variables selected in the MARS E_{50}/c_u model

listing the GCV score for a model with all BFs corresponding to that particular ANOVA function removed. The third column provides the standard deviation of this function. It also gives an indication of its relative importance to the overall model and can be interpreted in a manner similar to the standardized regression coefficient in a linear model. The fourth column gives the number of BFs comprising of the ANOVA function. The last column gives the particular input variables associated with the ANOVA function.

Fig. 7 gives the plot of the relative importance of the input variables, which is evaluated by the increase in the GCV value caused by removing the considered variables from the developed MARS model. The results indicates that the three most important variables influencing the determination of E_{50}/c_u are the calculated wall deflection δ_h^*, the system stiffness in logarithmic scale ln(S), and the soil relative shear strength ratio c_u/σ'_v.

Table 4 Basis functions and corresponding equations of MARS model for E_{50}/c_u

BF	Equation	BF	Equation
BF1	max(0, δ_h^* - 132)	BF15	BF2 × max(0, ln(S) - 7.313)
BF2	max(0, 132 - δ_h^*)	BF16	BF6 × max(0, T - 30)
BF3	max(0, ln(S) - 7.313)	BF17	BF6 × max(0, 30 - T)
BF4	max(0, 7.313 - ln(S))	BF18	BF9 × max(0, 54 - δ_h^*)
BF5	max(0, H_e - 17)	BF19	BF4 × max(0, γ - 17)
BF6	max(0, 17 - H_e)	BF20	BF4 × max(0, 17 - γ)
BF7	max(0, c_u/σ'_v - 0.25)	BF21	BF4 × max(0, c_u/σ'_v - 0.29)
BF8	max(0, 0.25 - c_u/σ'_v)	BF22	BF4 × max(0, 0.29 - c_u/σ'_v)
BF9	max(0, γ - 17)	BF23	BF7 × max(0, T - 30)
BF10	max(0, 17 - γ)	BF24	BF7 × max(0, 30 - T)
BF11	max(0, T - 30)	BF25	BF11 × max(0, γ - 17)
BF12	max(0, 30 - T)	BF26	BF11 × max(0, 17 - γ)
BF13	max(0, B - 40)	BF27	BF4 × max(0, H_e - 14)
BF14	max(0, 40 - B)	BF28	BF4 × max(0, 14 - H_e)

Table 4 lists the BFs and their corresponding equations for the developed MARS model. It is observed from Table 4 that interactions have occurred between BFs since exactly half of the basis functions are products of two spline functions (from BF15 to BF28). The presence of interactions suggests that these two models are not simply additive and that interactions play an important role in building accurate model for soil parameter identification. The equation of this optimal MARS model is given by

$$\begin{aligned} E_{50}/c_{\mathrm{u}} = {} & 290 - 1.97\times\mathrm{BF1} + 3.45\times\mathrm{BF2} - \\ & 133.26\times\mathrm{BF3} + 106.75\times\mathrm{BF4} + 8.61\times\mathrm{BF5} - \\ & 19.86\times\mathrm{BF6} - 1377\times\mathrm{BF7} + 1575\times\mathrm{BF8} - \\ & 17.64\times\mathrm{BF9} + 37.12\times\mathrm{BF10} + 15.80\times\mathrm{BF11} - \\ & 23.47\times\mathrm{BF12} + 1.2\times\mathrm{BF13} - 4.67\times\mathrm{BF14} + \\ & 0.67\times\mathrm{BF15} - 1.69\times\mathrm{BF16} + 2.16\times\mathrm{BF17} + \\ & 2.75\times\mathrm{BF18} - 19.37\times\mathrm{BF19} + 31.61\times\mathrm{BF20} - \\ & 372\times\mathrm{BF21} + 967\times\mathrm{BF22} - 53.95\times\mathrm{BF23} + \\ & 85\times\mathrm{BF24} - 2.42\times\mathrm{BF25} + 2.8\times\mathrm{BF26} + \\ & 3.23\times\mathrm{BF27} - 8.9\times\mathrm{BF28} \end{aligned} \quad (6)$$

Table 5 Summary of excavation case histories validating MARS E_{50}/c_u model

Case number and name	B (m)	T (m)	H_e (m)	$\frac{c_u}{\sigma'_v}$	$\delta_{h,M}^*$ (mm)	ln(S)	γ (kN/m^3)	μ_w	Target $\frac{E_{50}}{c_u}$ **	MARS predictions	References
1:Formosa	35	27	18.5	0.34	62	7.30	19.0	0.8	200	264	Ou *et al.* (1993)
2:Taiwan Power Company	60	13.5	14.7	0.30	63	6.65	19.0	0.9	150	212	Moh and Song (2013)
3: Shandao Temple	21.5	26.5	18.5	0.30	36.7	7.82	18.7	0.8	250	391	Fang (1987)
4: Xinyi planning zone	41	27	14.45	0.34	78	7.02	18.7	0.8	150	192	Fang *et al.*(2004)
5 Bugis MRT	21	35	18	0.25	135	8.18	16.5	0.9	150	164	Li (2002)
6 Lavender	24	16	15.7	0.25	32	7.96	17.0	0.8	150	172	Lim *et al.* (2003)
7 MRT line in Singapore	20	20	16	0.25	38.6	8.11	17.6	0.8	150	191	Goh *et al.* (2003)
8 Muni Metro Turnback	16	20.5	13.1	0.22	48	7.31	16.5	0.8	250	273	Koutsoftas *et al.* (2000)
9 Lurie	64	7.4	11.8	0.25	66	5.85	18.9	0.8	165	205	Kung *et al.* (2007)
10 Yanchang Road	18.1	15.5	15.2	0.30	65	5.77	18.0	0.9	190	183	Wang *et al.* (2005)
11 Pudian Road	20.4	15.5	16.5	0.30	71	6.12	18.0	0.9	190	132	Wang *et al.* (2005)
12 Shanghai Bank building	43	19.3	15.2	0.30	67.4	6.57	18.6	0.9	190	250	Xu *et al.* (2005)

∗As shown in Eq. (5), $\delta_{h,M} = \delta_h^* \times \mu_w$, $\delta_{h,M}$ is the measured wall deflection, mainly used as inputs for validation purposes based on case histories;

∗∗Herein target means that the values are from either lab/field tests and reported by the various authors or back analysis.

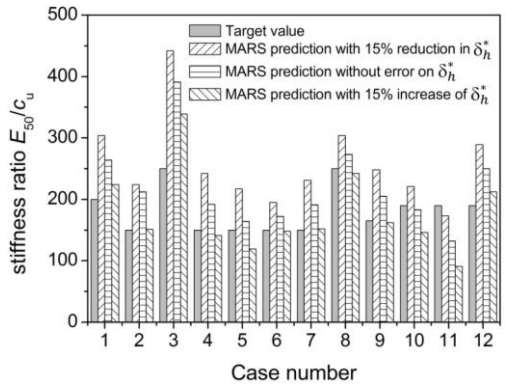

Fig. 8 Target and predicted E_{50}/c_u values by developed MARS model

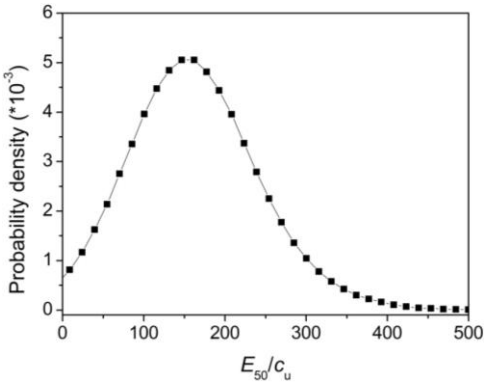

Fig. 9 Distribution of the predicted E_{50}/c_u values based on Eq. (6) for Bugis MRT

5. Excavation history validations on E_{50}/c_u model

To validate this proposed MARS model for soil parameter identification, a total of 12 well-documented excavation case histories from various countries as listed in Table 5 were analyzed. To visualize the quality of prediction, predicted stiffness ratio E_{50}/c_u values by MARS model are compared with the target values for the 12 cases listed in Table 5 and shown in Fig. 8. Fig. 8 also plots the range of E_{50}/c_u by varying δ_h^* by +15% and -15%. Table 5 and Fig. 8 indicate that the developed MARS model is able to predict reasonably well the soil stiffness ratios for the case histories considered, even with considerable variability in the wall deflection measurements.

Based on Eq. (6), Fig. 9 gives the plot of the probability density of E_{50}/c_u for a typical case (Bugis MRT station) derived from Monte Carlo Simulation with 1 000 000 iterations assuming that the coefficient of variation COV of both δ_h^* and c_u/σ'_v are 0.15. Both δ_h^* and c_u/σ'_v follow the normal distribution, the mean values of which are 150 and 0.25, respectively. The other five input variables are deterministic and the values can be found in Table 5. As can be seen from Fig. 9, the variation of E_{50}/c_u follows the normal distribution. The most probable E_{50}/c_u value is 147, very close to the target value of 150.

6. MARS model for ln(S)

A second MARS model was also developed for inverse parameter estimation of the wall system stiffness. This model will assist engineers to determine the appropriate wall size during the preliminary design phase. The same patterns as used for E_{50}/c_u model are adopted for training and testing of the MARS ln(S) model respectively. The optimal MARS model adopted 28 BFs of linear spline functions. For comparison, Fig. 10 plots the R^2 values of the testing data sets for the MARS ln(S) model with different BFs (from 14 to 48). The observed versus predicted 1:1 plots of ln(S) are shown in Fig. 11. Fig. 12 presents the histogram plots of the relative errors. It is obvious that most of the MARS estimations of the data patterns fell within

Table 6 Some typical training data for MARS ln(S) model

B (m)	T (m)	H_e (m)	c_u/σ'_v	E_{50}/c_u	δ_h^* (mm)	γ (kN/m^3)	Target ln(S)	MARS predicted ln(S)
40	25	20	0.34	100	95	19.0	8.176	8.319
30	25	20	0.34	100	110	17.0	7.313	7.559
30	30	20	0.34	100	115	17.0	8.176	8.120
30	30	14	0.34	100	98	17.0	8.176	8.169
40	25	20	0.34	200	68	19.0	8.176	8.109
30	30	17	0.34	200	58	19.0	8.846	8.721
30	30	20	0.25	200	86	19.0	8.846	9.153
40	30	20	0.29	200	87	19.0	8.846	8.849
40	30	20	0.21	200	115	19.0	8.846	9.029
50	25	14	0.29	200	81	17.0	8.176	8.251
40	25	20	0.34	300	57	19.0	8.176	8.092
30	30	20	0.34	300	63	19.0	8.176	8.001
30	25	20	0.34	300	70	17.0	7.313	7.499
30	30	20	0.29	300	77	19.0	8.176	8.048
40	25	17	0.25	300	72	19.0	8.176	8.235
30	30	17	0.25	300	83	19.0	8.176	8.145
30	30	11	0.29	300	54	19.0	7.313	7.315
40	25	17	0.25	300	142	19.0	6.097	5.856
40	30	11	0.21	300	93	17.0	8.176	8.030
40	30	17	0.25	300	181	19	6.097	6.142
30	30	14	0.34	300	151	15.0	6.097	5.951
40	30	20	0.25	300	202	19.0	6.097	6.044
30	30	11	0.34	400	26	19.0	8.846	8.699
30	30	17	0.34	400	41	19.0	8.846	8.810
40	30	20	0.34	400	75	19.0	7.313	7.332
40	30	17	0.34	400	68	19.0	7.313	7.351
30	30	11	0.29	400	45	19.0	7.313	7.260
30	30	17	0.29	400	61	19.0	8.176	8.070
40	35	17	0.25	400	123	19.0	7.313	7.399
40	30	14	0.25	400	90	19.0	7.313	7.292

Table 7 Some typical testing data for MARS ln(S) model

B (m)	T (m)	H_e (m)	c_u/σ'_v	E_{50}/c_u	δ_h^* (mm)	γ (kN/m^3)	Target ln(S)	MARS predicted ln(S)
30	30	20	0.34	100	106	19.0	8.176	8.151
30	30	20	0.29	100	122	19.0	8.176	8.310
40	25	17	0.34	100	114	19.0	7.313	7.012
50	25	20	0.34	100	136	17.0	7.313	7.357
30	30	20	0.29	200	75	19.0	8.846	8.904
30	25	17	0.34	200	78	17.0	7.313	7.281
50	25	17	0.29	100	151	17.0	7.313	7.381
50	25	20	0.29	200	116	17.0	7.313	7.442
40	30	11	0.34	200	64	19.0	7.313	7.441
30	25	17	0.21	200	126	17.0	7.313	7.442
30	25	20	0.29	200	150	17.0	6.097	5.955

Table 7 Continued

B (m)	T (m)	H_e (m)	c_u/σ'_v	E_{50}/c_u	δ_h^* (mm)	γ (kN/m^3)	Target ln(S)	MARS predicted ln(S)
40	35	17	0.34	200	128	17.0	7.313	7.337
40	25	17	0.29	300	63	19.0	8.176	8.004
30	30	14	0.34	300	54	19.0	8.176	8.219
40	25	20	0.34	300	94	19.0	6.097	6.075
40	35	20	0.25	400	147	19.0	7.313	7.297

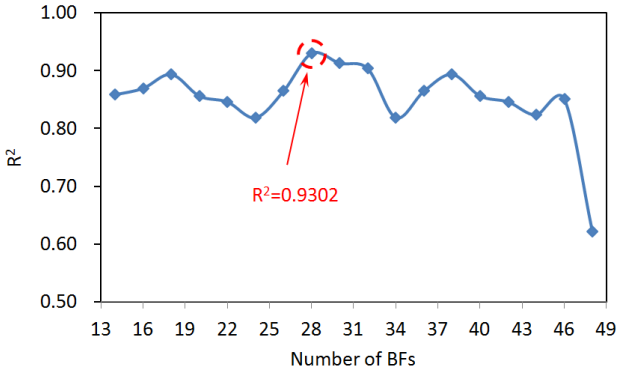

Fig. 10 R^2 for different number of BFs for ln(S) model

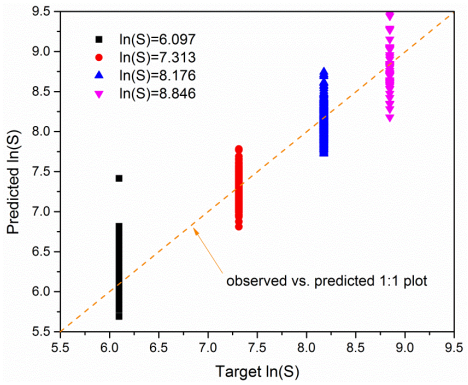

Fig. 11 Observed vs. predicted 1:1 plots of ln(S)

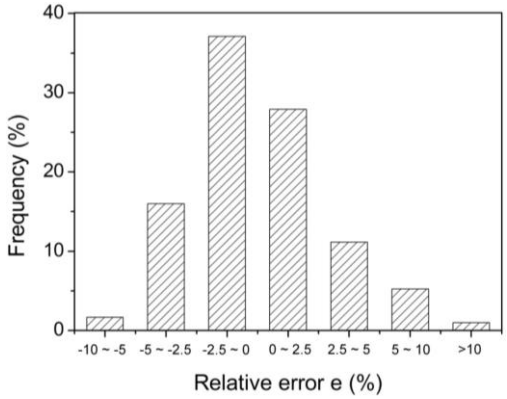

Fig. 12 Histogram of relative errors for MARS ln(S) model

±10% of the target values. Some typical training and testing data sets together with the MARS predictions are listed in Tables 6 and 7, respectively.

Table 8 lists the BFs and their corresponding equations

Table 8 Basis functions and corresponding equations of MARS ln(S) model

BF	Equation	BF	Equation
BF1	max(0, 46 - δ_h^*)	BF15	max(0, 118 - δ_h^*)
BF2	max(0, c_u/σ'_v - 0.25)	BF16	BF13 × max(0, E_{50}/c_u - 200)
BF3	max(0, 0.25 - c_u/σ'_v)	BF17	BF13 × max(0, 200 - E_{50}/c_u)
BF4	max(0, E_{50}/c_u - 300)	BF18	max(0, δ_h^* - 46) × max(0, E_{50}/c_u - 200)
BF5	max(0, 300 - E_{50}/c_u)	BF19	max(0, T - 30)
BF6	max(0, δ_h^* - 46) × max(0, H_e - 14)	BF20	max(0, 30 - T)
BF7	max(0, γ - 17)	BF21	BF13 × max(0, T - 30)
BF8	max(0, 17 - γ)	BF22	BF13 × max(0, 30 - T)
BF9	max(0, δ_h^* - 46) × max(0, 30 - T)	BF23	max(0, 190 - δ_h^*)
BF10	max(0, B - 40)	BF24	BF2 × max(0, δ_h^* - 74)
BF11	max(0, 40 - B)	BF25	BF2 × max(0, 74 - δ_h^*)
BF12	max(0, H_e - 17)	BF26	BF23 × max(0, 200 - E_{50}/c_u)
BF13	max(0, 17 - H_e)	BF27	BF5 × max(0, γ - 17)
BF14	max(0, δ_h^* - 118)	BF28	BF5 × max(0, 17 - γ)

for the developed MARS $\ln(S)$ model. It is observed from Table 8 that interactions have occurred between BFs since exactly 12 out of the 28 BFs are products of two spline functions. The presence of interactions suggests that these two models are not simply additive and that interactions play an important role in building MARS $\ln(S)$ model. The equation of this optimal MARS model is given by

$$\begin{aligned}\ln(S) = {} & 7.055 + 0.038\times BF1 - 16.977\times BF2 + \\ & 17.522\times BF3 - 0.004\times BF4 + 0.007\times BF5 - \\ & 0.0007\times BF6 - 0.318\times BF7 + 0.439\times BF8 - \\ & 0.0004\times BF9 + 0.024\times BF10 - 0.046\times BF11 + \\ & 0.149\times BF12 - 0.225\times BF13 - 0.007\times BF14 + \\ & 0.03\times BF15 - 0.0002\times BF16 + 0.0003\times BF17 + \\ & 2\times10^{-5}\times BF18 + 0.1\times BF19 - 0.152\times BF20 - \\ & 0.013\times BF21 + 0.015\times BF22 + 0.010\times BF23 + \\ & 0.040\times BF24 + 0.259\times BF25 + 7\times10^{-5}\times BF26 + \\ & 0.0007\times BF27 - 0.0008\times BF28\end{aligned} \quad (7)$$

7. Validations on $\ln(S)$ model

The same excavation case histories as used for validating the E_{50}/c_u model are adopted for verifying the

Table 9 Summary of excavation case histories validating MARS ln(S) model

Case No	Case name	B (m)	T (m)	He (m)	$\frac{c_u}{\sigma'_v}$	$\frac{E_{50}}{c_u}$	$\delta_{h,M}$ (mm)	γ (kN/m3)	μw	Target ln(S)	MARS predicted ln(S)	References
1	Formosa	35	27	18.5	0.34	200	62	19.0	0.8	7.30	7.142	Ou *et al.* (1993)
2	Taiwan Power Company	60	13.5	14.7	0.30	150	63	19.0	0.9	6.65	7.786	Moh and Song (2013)
3	Shandao Temple	21.5	26.5	18.5	0.30	250	36.7	18.7	0.8	7.82	8.761	Fang (1987)
4	Xinyi planning zone	41	27	14.45	0.34	150	78	18.7	0.8	7.02	7.201	Fang *et al.* (2004)
5	Bugis MRT	21	35	18	0.25	150	135	16.5	0.9	8.18	8.054	Li (2002)
6	Lavender	24	16	15.7	0.25	150	32	17.0	0.8	7.96	9.729	Lim *et al.* (2003)
7	MRT line in Singapore	20	20	16	0.25	150	38.6	17.6	0.8	8.11	9.343	Goh *et al.* (2003)
8	Muni Metro Turnback	16	20.5	13.1	0.22	250	48	16.5	0.8	7.31	8.253	Koutsoftas *et al.* (2000)
9	Lurie	64	7.4	11.8	0.25	165	66	18.9	0.8	5.85	7.440	Kung *et al.* (2007)
10	Yanchang Road	18.1	15.5	15.2	0.30	190	65	18.0	0.9	5.77	5.891	Wang *et al.* (2005)
11	Pudian Road	20.4	15.5	16.5	0.30	190	71	18.0	0.9	6.12	5.575	Wang *et al.* (2005)
12	Shanghai Bank building	43	19.3	15.2	0.30	190	67.4	18.6	0.9	6.57	7.218	Xu *et al.* (2005)

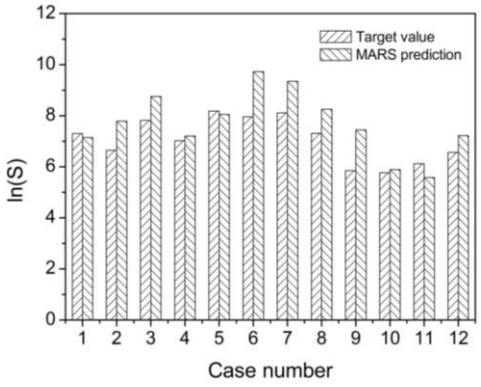

Fig. 13 Target and predicted ln(S) values by developed MARS model

developed MARS ln(S) model. The MARS predicted ln(S) values are compared with the target ones for cases listed in Table 9 and shown in Fig. 13. Table 9 and Fig. 13 indicate that the developed MARS model is able to provide reasonable estimates of the wall stiffness for the case histories considered.

8. Conclusions

This paper presents two MARS models developed for identifying soil parameters and configuring system stiffness in braced excavations based on field observation of maximum wall deflections. The MARS E_{50}/c_{u} model can relate the soil relative stiffness ratio to influencing parameters including the excavation geometries, soil shear strength ratio, unit weight, and the wall stiffness. The developed MARS ln(S) model provides estimates of the suitable wall stiffness based on a user-defined allowable wall deflection, thus saves design time by eliminating unsuitable wall configurations early in the design process. Well documented case histories from various countries validating the reliability of the proposed MARS models are given for a wide variety of wall and soil conditions.

It should be noted that the focus of this paper is on the proposed MARS methodology to identify soil parameters and configure system stiffness in braced excavations, and thus its application is limited to the soil deposits that can be modelled with the set of soil parameters used in this study. Furthermore, as the hypothetical cases to develop the MARS models assume a single layer of soft clay, consequently, the proposed method may not be applicable to excavations in heterogeneous or layered clay deposits or other ground types such as the sand and the stiff clays.

Acknowledgements

The corresponding author is grateful to the support by the National Natural Science Foundation of China (No. 51608071), and the Advanced Interdisciplinary Special Cultivation program (No. 106112017CDJQJ208850).

References

Attoh-Okine, N.O., Cooger, K. and Mensah, S. (2009), "Multivariate adaptive regression spline (MARS) and hinged hyper planes (HHP) for doweled pavement performance modeling", *Construct. Build. Mater.*, **23**(9), 3020-3023.

Brinkgreve, R.J.B., Broere, W. and Watermanm, D. (2006), *PLAXIS version 8.5 Manual*, AA Balkema, Rotterdam, The Netherlands.

Calvello, M. and Finno, R.J. (2004), "Selecting parameters to optimize in model calibration by inverse analysis", *Comput. Geotech.*, **31**(5), 411-425.

Chiu, C.F., Yan, W.M. and Yuen, K.V. (2012), "Estimation of water retention curve of granular soils from particle size distribution-a Bayesian probabilistic approach", *Can. Geotech. J.*, **49**(9), 1024-1035.

Clough, G.W. and O'Rourke, T.D. (1990), "Construction induced movements of in situ walls", *Proceedings of the Specialty Conference on Design and Performance of Earth Retaining Structures*, Ithaca, New York, U.S.A., June.

Fang, M.L. (1987), "A deep excavation in Taipei Basin", *Proceedings of the 9th Southeast Asian Geotechnical Conference*, Bangkok, Thailand, December.

Fang, T.C., Tsai, Y.Y., Su, T.C., Tsung, P. and Seeley, P. (2004), "A

case study on time-dependent displacement of diaphragm wall induced by creep of soft clay", *Proceedings of the 5th Cross-Strait Geotechnics Seminars*, Taipei, Taiwan, November.

Friedman, J.H. (1991), "Multivariate adaptive regression splines", *Ann. Stat.*, **19**, 1-67.

Gioda, G. (1985), "Some remarks on back analysis and characterization problems in geomechanics", *Proceedings of the 5th International Conference on Numerical Methods in Geomechanics*, Nagoya, Japan, April.

Goh, A.T.C., Wong, K.S., Teh, C.I. and Wen, D. (2003), "Pile response adjacent to braced excavation", *J. Geotech. Geoenviron. Eng.*, **129**(4), 383-386.

Goh, A.T.C. and Zhang, W.G. (2014), "An improvement to MLR model for predicting liquefaction-induced lateral spread using multivariate adaptive regression splines", *Eng. Geol.*, **170**, 1-10.

Goh, A.T.C., Zhang, W.G., Zhang, Y.M., Xiao, Y. and Xiang, Y.Z. (2018), "Determination of EPB tunnel-related maximum surface settlement: A multivariate adaptive regression splines approach", *Bull. Eng. Geol. Environ.*, **77**(2), 489-500.

Goh, A.T.C., Zhang, Y.M., Zhang, R.H., Zhang, W.G. and Xiao, Y. (2017), "Evaluating stability of underground entry-type excavations using multivariate adaptive regression splines and logistic regression", *Tunn. Undergr. Sp. Technol.*, **70**, 148-154.

Hashash, Y., Levasseur, S., Osouli, A., Finno, R. and Malecot, Y. (2010), "Comparison of two inverse analysis techniques for learning deep excavation response", *Comput. Geotech.*, **37**(3), 323-333.

Hastie, T., Tibshirani, R. and Friedman, J. (2009), *The Elements of Statistical Learning: Data Mining, Inference and Prediction*, Springer.

Jekabsons, G. (2010), "VariReg: A software tool for regression modelling using various modeling methods", Riga Technical University, <http://www.cs.rtu.lv/jekabsons>.

Ji, J., Zhang, C., Gui, Y., Lü, Q. and Kodikara, J. (2016), "New observations on the application of LS-SVM in slope system reliability analysis", *J. Comput. Civ. Eng.*, **31**(2), 06016002.

Juang, C.H., Luo, Z., Atamturktur, S. and Huang, H. (2013), "Bayesian updating of soil parameters for braced excavations using field observations", *J. Geotech. Geoenviron. Eng.*, **139**(3), 395-406.

Koutsoftas, D.C., Frobenius, P., Wu, C.L., Meyersohn, D. and Kulesza, R. (2000), "Deformations during cut-and cover construction of MUNI metro turnback project", *J. Geotech. Geoenviron. Eng.*, **126**(4), 344-359.

Kung, G.T.C., Hsiao, E.C.L. and Juang, C.H. (2007), "Evaluation of a simplified small-strain soil model for analysis of excavation-induced movements", *Can. Geotech. J.*, **44**(6), 726-736.

Lashkari, A. (2012), "Prediction of the shaft resistance of non-displacement piles in sand", *Int. J. Numer. Anal. Meth. Geomech.*, **37**(8), 904-931.

Lecampion, B., Constantinescu, A. and Nguyen Minh, D. (2002), "Parameter identification for lined tunnels in viscoplastic medium", *Int. J. Numer. Anal. Meth. Geomech.*, **26**(12), 1191-1211.

Levasseur, S., Malécot, Y., Boulon, M. and Flavigny, E. (2008), "Soil parameter identification using a genetic algorithm", *Int. J. Numer. Anal. Meth. Geomech.*, **32**(2), 189-213.

Levasseur, S., Malécot, Y., Boulon, M. and Lavigny, E. (2010), "Statistical inverse analysis based on genetic algorithm and principal component analysis: Applications to excavation problems and pressuremeter tests", *Int. J. Numer. Anal. Meth. Geomech.*, **34**(5), 471-491.

Li, W. (2001), "Braced excavation in old alluvium in Singapore", Ph.D. Thesis, Nanyang Technological University, Nanyang, Singapore.

Lim, K.W., Wong, K.S., Orihara, K. and Ng, P.B. (2003), "Comparison of results of excavation analysis using WALLUP, SAGE CRISP, and EXCAV97", *Proceedings of the Singapore Underground*, Nanyang, Singapore, November.

Miranda, T. (2007), "Geomechanical parameters evaluation in underground structures. Artificial intelligence, Bayesian probabilities and inverse methods", Ph.D. Thesis, University of Minho, Guimarães, Portugal.

Mirzahosseinia, M., Aghaeifarb, A., Alavic, A., Gandomic, A. and Seyednour, R. (2011), "Permanent deformation analysis of asphalt mixtures using soft computing techniques", *Expert Syst. Appl.*, **38**(5), 6081-6100.

Moh, Z.C. and Song, T.F. (2013), "Performance of diaphragm walls in deep foundation excavations", *Proceedings of the 1st International Conferences on Case Histories in Geotechnical Engineering*, St. Louis, Missouri, U.S.A., May.

Moreira, N., Miranda, T., Pinheiro, M., Fernandes, P., Dias, D., Costa, L. and Sena-Cruz, J. (2013), "Back analysis of geomechanical parameters in underground works using an Evolution Strategy algorithm", *Tunn. Undergr. Sp. Technol.*, **33**, 143-158.

Ou, C.Y., Hsieh, P.G. and Chiou, D.C. (1993), "Characteristics of ground surface settlement during excavation", *Can. Geotech. J.*, **30**(5), 758-767.

Ou, C.Y. and Tang, Y. (1994), "Soil parameter determination for deep excavation analysis by optimization", *J. Chin. Inst. Eng.*, **17**(5), 671-688.

Papon, A., Riou, Y., Dano, C. and Hicher, P.Y. (2011), "Single and multi-objective genetic algorithm optimization for identifying soil parameters", *Int. J. Numer. Anal. Meth. Geomech.*, **36**(5), 597-618.

Rechea, C., Levasseur, S. and Finno, R. (2008), "Inverse analysis techniques for parameter identification in simulation of excavation support systems", *Comput. Geotech.*, **35**(3), 331-345.

Samui, P. (2011), "Determination of ultimate capacity of driven piles in cohesionless soil: A multivariate adaptive regression spline approach", *Int. J. Numer. Anal. Meth. Geomech.*, **36**(11), 1434-1439.

Samui, P. and Karup, P. (2011), "Multivariate adaptive regression spline and least square support vector machine for prediction of undrained shear strength of clay". *Int. J. Appl. Metaheur. Comput.*, **3**(2), 33-42.

Wang, Z.W., Ng, C.W.W. and Liu, G.B. (2005), "Characteristics of wall deflections and ground surface settlements in Shanghai", *Can. Geotech. J.*, **42**(5), 1243-1254.

Xu, Z.H., Wang, W.D., Wang, J.H. and Shen, S.L. (2005), "Performance of deep excavation retaining wall in Shanghai soft deposit", *Lowland Technol. Int.*, **7**(2), 31-43.

Yan, W.M., Yuen, K.V. and Yoon, G.L. (2009), "Bayesian probabilistic approach for the correlations of compressibility index for marine clays", *J. Geotech. Geoenviron. Eng.*, **135**(12), 1932-1940.

Zarnani, S., El-Emam, M. and Bathurst, R.J. (2011), "Comparison of numerical and analytical solutions for reinforced soil wall shaking table tests", *Geomech. Eng.*, **3**(4), 291-321.

Zentar, R., Hicher, P. and Moulin, G. (2001), "Identification of soil parameters by inverse analysis", *Comput. Geotech.*, **28**(2), 129-144.

Zhang, C.S., Ji, J., Gui, Y.L., Kodikara, J., Yang, S.Q. and He, L. (2016), "Evaluation of soil-concrete interface shear strength based on LS-SVM", *Geomech. Eng.*, **11**(3), 361-372.

Zhang, W.G. and Goh, A.T.C. (2013), "Multivariate adaptive regression splines for analysis of geotechnical engineering systems", *Comput. Geotech.*, **48**, 82-95.

Zhang, W.G. and Goh, A.T.C. (2014), "Multivariate adaptive regression splines model for reliability assessment of serviceability limit state of twin caverns", *Geomech. Eng.*, **7**(4),

431-458.
Zhang, W.G. and Goh, A.T.C. (2015), "Nonlinear modeling using multivariate adaptive regression splines", *Comput. Concrete*, **16**, 569-585.
Zhang, W.G. and Goh, A.T.C. (2016a), "Evaluating seismic liquefaction potential using multivariate adaptive regression splines and logistic regression", *Geomech. Eng.*, **10**(3), 269-284.
Zhang, W.G. and Goh, A.T.C. (2016b), "Multivariate adaptive regression splines and neural network models for prediction of pile drivability", *Geosci. Front.*, **7**(1), 45-52.
Zhang, W.G. and Goh, A.T.C. (2018), "Reliability analysis of geotechnical infrastructures: Introduction", *Geosci. Front.*
Zhang, W.G., Goh, A.T.C. and Xuan, F. (2015), "A simple prediction model for wall deflection caused by braced excavation in clays", *Comput. Geotech.*, **63**, 67-72.
Zhao, B.D., Zhang, L.L., Jeng, D.S., Wang, J.H. and Chen, J.J. (2015), "Inverse analysis of deep excavation using differential evolution algorithm", *Int. J. Numer. Anal. Meth. Geomech.*, **39**(2), 115-134.

CC